Comput Mech (2011) 48:499–513
DOI 10.1007/s00466-011-0603-8

ORIGINAL PAPER

Application of triangular element invariants for geometrically nonlinear analysis of functionally graded shells

S. V. Levyakov · V. V. Kuznetsov

Received: 18 August 2010 / Accepted: 18 April 2011 / Published online: 12 May 2011

Abstract This paper is an attempt to construct a computationally effective curved triangular finite element for geometrically nonlinear analysis of elastic shear deformable shells fabricated from functionally graded materials. The focus is on the concise finite-element formulation under the demand of accuracy-simplicity trade-off. To this end, a non-conventional approach based on the invariants of the natural strains of fibers parallel to the element edges is used. The approach allows one to obtain algorithmic formulas for computing the stiffness matrix, gradient, and Hessian of the total strain energy of the finite element. Transverse shear deformation effects are taken into account using the first order shear deformation theory with the shear correction factor dependent on the material property distribution across the shell thickness. The performance of the proposed finite element is demonstrated using problems of functionally graded plates and shells under mechanical and thermal loads.

Keywords Functionally graded material · Shear deformable shell · Geometrical nonlinearity · Strain invariants · Finite element

1 Introduction

An important issue arising in the design of a structure is to determine the geometry and dimensions of the structural components to ensure that the structure withstands the expected loads during service. In some engineering applications where strength and reliability requirements are combined with stringent lightweight constraints, an optimum design can be developed by using composite materials with special thermo-mechanical properties.

In the recent years, much attention has been given to functionally graded materials (FGM) composed of two or more constituents, usually metal and ceramics, mixed in such a manner that the properties of the resulting material vary continuously and smoothly over the bulk of the solid. Historically, the concept of FGM was considered in the 1980s by a group of material scientists in Japan [1] to withstand severe temperature by combining high thermal resistance of the outer surface of a structure with high fracture resistance of its inner surface. Proposed initially as heat-shielding materials for space planes and fusion reactors, FGMs have now a broad range of applications including automotive, biomedical, mechanical, and naval engineering.

Of much practical interest are plate- and shell-like structures made of functionally graded materials whose properties vary continuously through the thickness only. In contrast to isotropic plates and shells, these structures exhibit pronounced membrane-bending coupling effects. Owing to variation of elastic properties across the thickness, the neutral surface in which fibers do not change in length upon bending is no longer at the middle surface. This implies, in particular, that tension or compression causes the functionally graded structure to bend. Behavior of functionally graded (FG) plates and shells under static, dynamic, and thermal loading conditions has been studied in the scientific literature using various deformation models of solid mechanics.

The simplest deformation model applied to analysis of thin functionally graded structures is based on the classical plate theory and small-displacement approximation. Chi and Chung [2,3] considered the linear problem of simply supported rectangular plates subjected to transverse loads and obtained double-series analytical solutions for various laws of elastic property distribution across the thickness.

S. V. Levyakov (✉) · V. V. Kuznetsov
Department of Engineering Mathematics,
Novosibirsk State Technical University,
630092 Novosibirsk, Russia
e-mail: stan-levyakov@yandex.ru

Navazi et al. [4] performed the displacement and stress analyses of rectangular FG plates in cylindrical bending and showed that, under certain loading conditions, behavior of FG plates cannot be modeled adequately using isotropic model even in the small-deflection range. It follows that averaging the elastic properties of the FG structure may lead to erroneous results. Approximate nonlinear analysis of rectangular thin FG plates undergoing large deflections in the von-Karman sense was performed by the energy method by Ghannadpour and Alinia [5]. Buckling and postbuckling of simply supported rectangular plates under mechanical and thermal loads were investigated by Shariat et al. [6,7] and Javaheri and Eslami [8,9] using double-series method. Yang and Shen [10] applied semi-analytical procedure to investigate nonlinear behavior of rectangular plates under various loading and boundary conditions. Using the von-Karman plate theory, Ma and Wang [11] studied axisymmetric nonlinear bending and postbuckling response of circular plates subjected to mechanical and thermal loading conditions by the shooting method. Najafizadeh and Eslami [12] obtained exact analytical solutions for the buckling problem of circular plates using Sander's nonlinear strain–displacement relations. Woo and Meguid [13] applied the von-Karman theory to the large-deflection analysis of FG plates and shallow shells under mechanical and thermal loads and obtained solution by the Fourier series method. The buckling and postbuckling behavior of cylindrical shells was studied by Huang and Han [14,15], Wu et al. [16], and Yang et al. [17] using the equations of the Donnell shell theory. Li and Batra [18] gave solution to the buckling problem of a three-layer thin cylindrical FG shell based on the Flugge shell equations.

A more accurate analysis of composite plates and shells is based on theories which take into account transverse shear deformation. Praveen and Reddy [19] performed a finite-element analysis of ceramic–metal plates subjected to steady temperature field using the first-order shear deformation theory. Croce and Venini [20] proposed a locking-free family of finite elements for linear analysis of Reissner–Mindlin plates. Navazi and Haddadpour [21] obtained an exact analytical solution for cylindrical bending of shear deformable plates governing large displacements under transverse and in-plane loads. They found that nonlinear analyses based on the classical plate theory and first-order deformation theory give very close results for displacements, but different stress distributions near the boundaries of FG plates. Nonlinear behavior, buckling, and postbuckling of moderately thick plates under thermal and mechanical loads were studied by Wu [22], Prakash et al. [23,24], Wu et al. [25], Shen [26,27], Park and Kim [28], Audogdy [29], and Nosier and Fallah [30]. Santos et al. [31] proposed a semi-analytical finite-element model for linear analysis of cylindrical shells. Ganesan et al. [32,33] studied linear buckling behavior and vibration of functionally graded shells of revolution by the semi-analytical finite element method. Zhao and Liew [34] proposed a mesh-free method for nonlinear analysis of shallow shells based on a modified version of Sander's shell theory restricted to moderate rotations. Motivated by the lack of nonlinear elements, Reddy and Arciniega [35] developed a tensor-based finite element for analysis of FG shells. To avoid locking, they used high order polynomials to approximate the displacement fields, which resulted in a large number of degrees of freedom per element. It is worth noting that most of the studies based on the first-order shear deformation theory adopt a value of 5/6 for the shear correction factor thus ignoring the effect of inhomogeneous structure of the functionally graded plates across the thickness. This issue was considered by Nguen et al. [36] who investigated the dependence of the shear correction factor on the properties of FGMs and obtained a series solution governing linear response of rectangular plates under static transverse mechanical loads.

Application of higher-order shear deformation theories to stress, buckling, and vibration analysis of thick functionally graded plates can be found in Reddy [37], Najafizadeh and Heydari [38]. An accurate stress analysis using three-dimensional relations of the theory of elasticity was performed by Li et al. [39,40] for circular plates under axisymmetric transverse loads and Batra et al. [41,42] for rectangular plates.

Review of the literature shows that mechanics of functionally graded shell-like structures have been studied extensively using the classical problems of plates and shells of simple geometry. It should be noted, however, that most of the studies addressing nonlinear behavior are based on the simplified theories that describe nonlinear effects only in a quadratic approximation. Little appears to have been done in developing finite elements for nonlinear analysis of shells made of functionally graded materials.

The aim of this paper is to develop a simple and computationally effective curved triangular finite element for nonlinear analysis of functionally graded elastic shells undergoing arbitrarily large displacements and rotations. The focus is on the concise formulation of the finite element. To this end, an invariant-based approach applied previously to develop finite elements of isotropic and transversely isotropic shells [43–45] is employed. As in the natural-mode method proposed by Argyris [46–48], the strain energy of triangular element is determined by three natural strains of fibers parallel to the triangle edges. A set of special invariants of the natural strains is used to determine the stain energy of the triangular element and compute the stiffness matrix, gradient, and Hessian of the total strain energy of the finite element. An obvious benefit of the natural strain invariants is that no local coordinate systems associated with the finite element are needed and, hence, computational work on the coordinate transformation is eliminated.

The kinematics of the element under arbitrarily large rotations is described via the concept of kinematic group, a geometrical object comprising nodal position vectors and unit vectors (directors). The kinematic group is briefly reviewed in Sect. 3.

Numerical examples are chosen to demonstrate performance of the element and investigate the effect of material property distribution on response of FG plates to applied mechanical and thermal loads.

2 Basic assumptions

We consider a shell finite element cut by three planes normal to the shell middle surface. The formulation of the curved triangular finite element presented below is based on the following assumptions.

1. Shell material exhibits perfectly elastic behavior.
2. Strains are small compared to unity, but arbitrarily large displacements and rotations are allowed.
3. Transverse shear deformation is taken into account using the first-order shear deformation theory.
4. Physical and mechanical properties of the material are distributed over the shell thickness according to power law.
5. The edges of the finite element are planar nearly circular arcs before and after deformation.
6. The membrane strains of the fibers parallel to the element edges are constant.
7. The area of a curved triangular element is equal to the area of a planar triangle whose side lengths are equal to those of the curved triangle.

Assumptions 1–3 are commonly used in the geometrically nonlinear analysis of plates and shells.

Assumption 4 refers to the approximation of the material property variation over the bulk of the shell. We confine our attention to functionally graded materials fabricated by mixing two material phases with different properties. Usually metal and ceramic phases are mixed in such a manner that their volume fractions denoted by V_m and V_c, respectively, grade in the thickness direction. It is common practice to approximate continuous volume fraction distribution across the shell thickness by the power law:

$$V_c = (0.5 + z/h)^n, \quad V_c + V_m = 1, \quad n \geq 0. \tag{2.1}$$

Here n is the volume fraction index, z is the coordinate reckoned from the shell middle surface, and h is the shell thickness. To approximate variation of any material property denoted by P, it is reasonable to assume that the same simple rule of mixture holds:

$$P(z) = P_m V_m + P_c V_c. \tag{2.2}$$

Relations (2.1) and (2.2) can be combined to give

$$P(z) = P_m + (P_c - P_m)(0.5 + z/h)^n. \tag{2.3}$$

Varying the exponent n in (2.3), one obtains various distribution profiles of properties across the thickness. According to (2.3), the bottom surface of the shell ($z = -h/2$) is metal rich and the top surface ($z = h/2$) is ceramic rich. Two limit cases follow from approximation (2.3): isotropic ceramic shell for $n = 0$ and isotropic metal shell as $n \to \infty$. Other models for evaluating the properties of FGMs can be found in [41,49].

Assumptions 5 and 6 are used to construct the triangular shell element. Assumption 5 concerns the nature of deformation of reasonably small element and states that pure bending is the principal part of its deformation. This makes it possible to describe finite rotations within the elements and enhance geometrically nonlinear capabilities of the element without increasing the number of elemental degrees of freedom. The validity of these assumptions were supported by extensive numerical data reported in [43–45].

Finally, Assumption 7 is adopted to take into account the shell metrics. It introduces a correction to the faceted element approach where the side lengths and area of the element are smaller compared to those of the real curved element.

3 Kinematics of the shell finite element

In the present approach, as in the natural-mode finite element method proposed by Argyris (see e.g. [47,48]), a finite element is looked upon as an individual mechanical object, not just as a region of the shell body where differential relations involved in the strain-energy functional are approximated via shape functions. To describe kinematics of the finite element in the presence of large displacements and rotations, a certain geometrical object referred to as kinematic group is used [50].

We consider three nodes i, j, and k lying on the shell middle surface and denote their position vectors by $\boldsymbol{r}_i, \boldsymbol{r}_j$, and $\boldsymbol{r}_k$, respectively. At these nodes, we determine three unit vectors $\boldsymbol{n}_i, \boldsymbol{n}_j$, and $\boldsymbol{n}_k$ normal to the middle surface of the undeformed shell (Fig. 1).

Definition 1 A geometrical object comprising the nodal points and adjoined vectors (directors) is called a kinematic group (KG) of the shell.

Configuration of the KG is determined by the distances between the nodes and relative position of the vectors $\boldsymbol{r}_m$ and $\boldsymbol{n}_m$. To describe the initial configuration of the group, we introduce nine quantities calculated by the formulas

$$e_i = \sqrt{(\boldsymbol{r}_k - \boldsymbol{r}_j)^2}, \quad \psi_{1j} = \boldsymbol{n}_j(\boldsymbol{r}_k - \boldsymbol{r}_j), \; \psi_{2k} = \boldsymbol{n}_k(\boldsymbol{r}_k - \boldsymbol{r}_j). \tag{3.1}$$

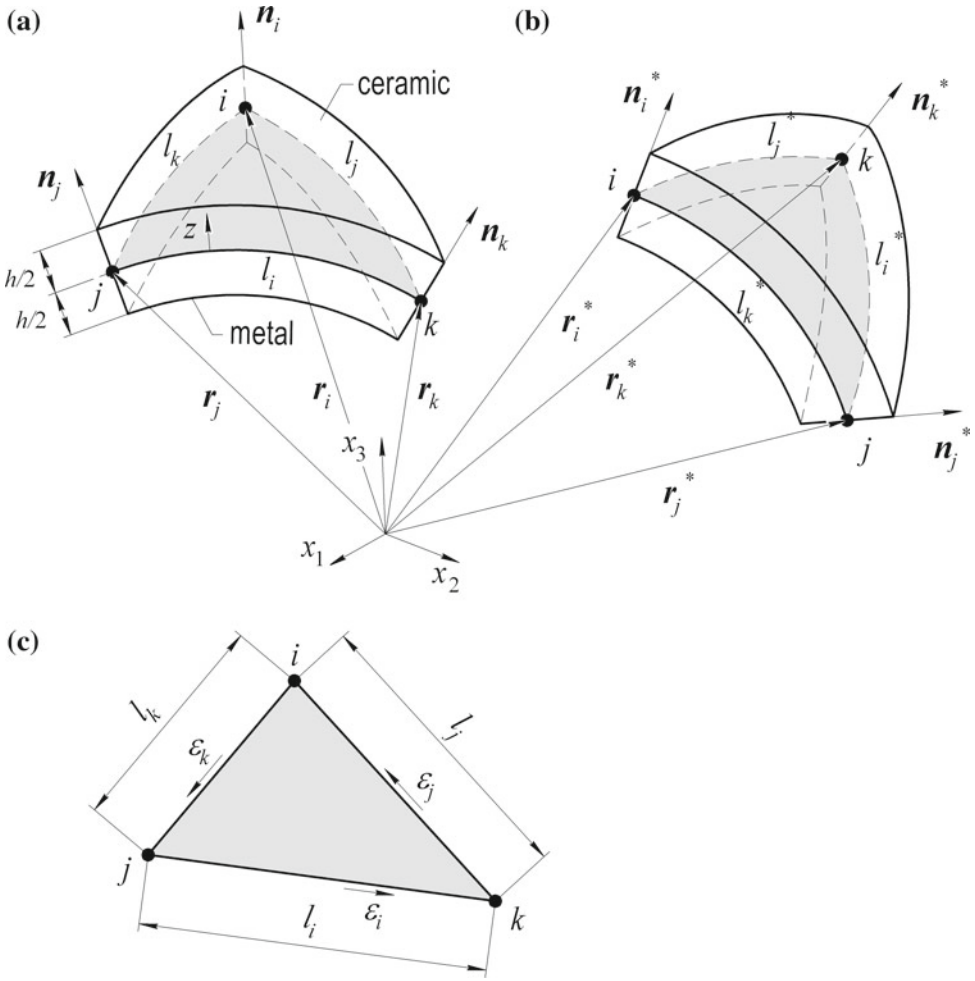

Fig. 1 Kinematic group and shell element: **a** undeformed state; **b** deformed state; **c** isometric triangle

Here and below, the subscripts i, j, and k obey the rule of cyclic permutation. It follows from (3.1) that the quantities e_i are the distances between the nodes and the two quantities ψ_{1i} and ψ_{2i} can be used to determine the orientation of the vector $\boldsymbol{n}_i$ with respect to the plane passing through the nodes.

Now we consider a new, deformed state of the shell. Obviously, deformation of the shell brings the kinematic group to new configuration described by the parameters

$$e_i^* = \sqrt{(\boldsymbol{r}_k^* - \boldsymbol{r}_j^*)^2}, \quad \psi_{1j}^* = \boldsymbol{n}_j^*(\boldsymbol{r}_k^* - \boldsymbol{r}_j^*), \\ \psi_{2k}^* = \boldsymbol{n}_k^*(\boldsymbol{r}_k^* - \boldsymbol{r}_j^*), \tag{3.2}$$

where the asterisk denotes the quantities that refer to the deformed state. To measure changes in the configuration of the KG, we determine the kinematic-group strains as the differences between the corresponding quantities (3.2) and (3.1). It was shown in [50] that the quantities (3.2) retain their values upon rigid-body motion including arbitrarily large rotations, which implies that the kinematic-group strains remain invariant under rigid body motion of the shell. This important property is used in the derivation of the finite element.

Definition 2 A finite element is associated with the kinematic group if the strains at each point of the element are continuous functions of the kinematic-group strains.

Once the strains within a finite element are interpolated in terms of the kinematic-group strains taken as the nodal parameters, this element automatically meets the necessary convergence criterion. Indeed, the kinematic-group strains and, hence, strains within the element do not occur under rigid-body motion. The strains occur in the associated finite element if and only if at least one kinematic-group strain is nonzero. Thus, the KG can be thought of as a framework of the finite element.

We consider the question of degrees of freedom of the kinematic-group. As follows from (3.2), changes in the configuration of the kinematic group are determined by variations in the nodal vectors $\boldsymbol{r}_m^*$ and $\boldsymbol{n}_m^*$ ($m = 1, 2, 3$). Each nodal position vector $\boldsymbol{r}_m^*$ has three independent variations δx_{1m}^*, δx_{2m}^*, and δx_{3m}^*, where x_{nm}^* is the nth coordinate of the mth node. In accordance with the Reissner–Mindlin assumptions, we require that the vectors $\boldsymbol{n}_m^*$ be inextensible, i.e. $(\boldsymbol{n}_m^*)^2 = 1$, but not necessarily normal to the shell

middle surface. Under this constraint, the vector $\boldsymbol{n}_m^*$ has only two independent variations $\delta\omega_{1m}$ and $\delta\omega_{2m}$ having the meaning of rotations. Thus, geometrical variability of the kinematic group is characterized by 5 independent variations per node, a total of 15 variations referred to as degrees of freedom. These variations comprise six rigid-body motions and nine purely straining modes represented by changes in the quantities (3.2).

4 Invariants of strain tensors

In this section, we briefly review basic relations for the strain–tensor invariants of the shear deformable shell considered in [45] which are used below to formulate the finite-element model of the functionally graded shell.

Independent of the reference frame chosen, invariants of the strain and stress tensors are objective characteristics of the stress–strain state at a point of a solid. They have theoretical significance and appear in almost every book on the theories of elasticity and plasticity. To the authors' knowledge, however, the invariants have so far seen little use in developing numerical methods for analysis of deformable solids. An example can be found in the paper of Zhao and Chen [51] where the first strain invariant was used to derive a plate bending finite element. In previous works of the authors [43–45], the strain invariants were employed to formulate triangular finite elements of isotropic shells based on the Kirchhoff–Love and Reissner–Mindlin assumptions.

We denote the side lengths of the curved triangular element by l_m ($m = 1, 2, 3$). By Assumption 7, we consider the corresponding planar triangle having the same side lengths which we call the isometric triangle (see Fig. 1c). For a triangular domain, it is convenient to introduce three special coordinates measured along three nonparallel directions rather than two curvilinear coordinates. As these directions, three directions determined by the triangle sides are natural to use. Given three normal strains measured in three nonparallel directions, one can always obtain all components of the strain tensor. This well-known idea is implemented in strain gage rosettes used in experimental investigation of the strains in structures. It should be noted that the concept of natural coordinates which are "in harmony" with triangles was first introduced by Argyris and co-workers into the finite element theory (e.g. [47]).

We consider the following invariants which describe a strained state of a shell subject to the assumptions of the first-order shear deformation theory [45] (summation over $m, n = 1, 2, 3$):

$$
\begin{aligned}
&I_\varepsilon = 2(aa_m\varepsilon_m - 2a_m^2\varepsilon_m), \quad I_{\varepsilon\varepsilon} = (a_m\varepsilon_m)^2 - 2a_m^2\varepsilon_m^2,\\
&I_\kappa = 2(aa_m\kappa_m - 2a_m^2\kappa_m), \quad I_{\kappa\kappa} = (a_m\kappa_m)^2 - 2a_m^2\kappa_m^2,\\
&I_\Gamma = 2(aa_m\Gamma_m - 2a_m^2\Gamma_m),\\
&I_{\varepsilon\kappa} = (a_m\varepsilon_m)(a_n\kappa_n) - 2a_m^2(\varepsilon\kappa)_m.
\end{aligned}
\tag{4.1}
$$

Here a_m are the metric coefficients which are assumed to be constant within the element, ε_m and κ_m are the strain and curvature change of the mth edge of the triangle, γ_m is the transverse shear strain in the mth direction, Γ_m is the squared shear strain determined as $\Gamma_m = \gamma_m^2$, and $(\varepsilon\kappa)_m = \varepsilon_m\kappa_m$, where no summation is performed over m. It is worth noting that the combined invariant introduced in [45] is written here in a different form. Namely, a factor of 2 is omitted so that the second invariants $I_{\varepsilon\varepsilon}$ and $I_{\kappa\kappa}$ can be obtained as particular cases from the expression for $I_{\varepsilon\kappa}$.

With allowance for Assumption 7, the metric coefficients are given by (summation over $m = 1, 2, 3$)

$$
a_m = \frac{l_m^2}{4F}, \quad a = \frac{l_m l_m}{4F}, \quad F = \frac{1}{4}\left[(l_m l_m)^2 - 2l_m^2 l_m^2\right]^{1/2},
\tag{4.2}
$$

where F is the area of the triangle which lies on the shell middle surface. The invariant $I_{\varepsilon\kappa}$ in (4.1), which we call the combined invariant, takes into account membrane-bending coupling of the FG shell with nonsymmetric distribution of mechanical properties about the shell middle surface.

The strain invariants (4.1) and, hence, the strain state of the shell element are determined by the one-dimensional quantities ε_m, κ_m, and Γ_m having clear physical meaning of the membrane strain, curvature change, and squared transverse shear strain, respectively, determined for the mth direction. These quantities can easily be approximated using one-dimensional solutions of the beam bending problems (see [45]). The next step is to relate one-dimensional strains ε_m, κ_m, and Γ_m to the nodal parameters of the kinematic group described in Sect. 3.

5 Expressions for strains

Below, we give strain relations for the side opposite to the node i of the triangular element (see Fig. 1). For the other sides, similar relations can be obtained by cyclic permutation of indices i, j, and k. A detailed derivation of these relations can be found in [44]. Using Assumptions 5 and 6, we obtain the following expressions for the membrane strain ε_i, curvature change κ_i, and transverse shear strain γ_i (see [45]):

$$
\begin{aligned}
&\varepsilon_i = \frac{e_i^*}{l_i}\cdot\frac{\sin^{-1}(\Delta\chi_i^*)}{\Delta\chi_i^*} - 1,\\
&\kappa_i = \frac{1}{l_i}(\vartheta_{2k} - \vartheta_{1j}) + \frac{\eta_{i1}}{l_i}(\vartheta_{2k} + \vartheta_{1j})(L_k - L_j),\\
&\gamma_i = \eta_{i2}(\vartheta_{2k} + \vartheta_{1j})
\end{aligned}
\tag{5.1}
$$

where

$$\Delta\chi_i^* = \frac{\chi_{2k}^* - \chi_{1j}^*}{2}, \quad \chi_{2k}^* = \frac{\psi_{2k}^*}{e_i^*}, \quad \chi_{1j}^* = \frac{\psi_{1j}^*}{e_i^*}, \qquad l_i = e_i \frac{\sin^{-1}(\Delta\chi_i)}{\Delta\chi_i} \tag{5.2}$$

$$\vartheta_{2k} = \sin^{-1}(\chi_{2k}^*) - \sin^{-1}(\chi_{2k}), \qquad \vartheta_{1j} = \sin^{-1}(\chi_{1j}^*) - \sin^{-1}(\chi_{1j}), \tag{5.3}$$

$$\eta_{i1} = \frac{3}{1+\eta_{i3}}, \quad \eta_{i2} = \frac{1}{6}\eta_{i1}\eta_{i3}, \quad \eta_{i3} = \frac{12 D_1}{C_\Gamma l_i^2}. \tag{5.4}$$

Here the asterisk denotes the quantities which refer to a deformed state, ϑ_{1j} and ϑ_{2k} are the pure deformation rotations at the ends of the ith edge, L_i are the area coordinates (see e.g. [52]), and D_1 and C_Γ are the rigidity factors given in Sect. 6. The expression for the curvature change κ_i and transverse shear strain γ_i are given by the solution of the bending problem of the Timoshenko beam subjected to end rotations ϑ_{1j} and ϑ_{2k}. The first term in the expression for κ_i represents the pure bending, which, by Assumption 5, is the principal part of the beam deformation. The second term takes into account the transverse shear force that occurs if the end rotations are "unbalanced". It should be noted that $\eta_{i1} \to 3$ as $C_\Gamma \to \infty$. It follows that convergence to the Kirchhoff–Love shell solutions is achieved and shear locking is eliminated completely. Relations (5.1) are valid for large ϑ_{1j} and ϑ_{2k} provided the sum of these quantities is small. In the case of pure bending where $\vartheta_{1j} + \vartheta_{2k} = 0$, one obtains $\varepsilon_i = 0, \gamma_i = 0$, and $\kappa_i = (\vartheta_{2k} - \vartheta_{1j})/l_i$.

Thus, the strains of the elemental edge ε_i, κ_i, and γ_i (5.1) have been expressed in terms of the quantities which determine a deformed configuration of the kinematic group e_i^*, ψ_{1j}^*, and ψ_{2k}^*(3.2).

To formulate equations for determining equilibrium states of the shell finite-element model, it is necessary to calculate the variations in the strain energy. The variations in the strains (5.1) are related to variations in e_i^*, ψ_{1j}^*, and ψ_{2k}^* which in turn are expressed in terms of independent variations in the vectors determining the kinematic group discussed in Sect. 3. The direct derivation of the variations in the strains (5.1) leads to intractable cumbersome expressions. In the context of numerical computations, however, we are more interested in an algorithmic procedure for calculating the coefficients of variations rather than in the analytical expressions. To facilitate the calculations, we introduce three "variation levels" of variable parameters represented by the vectors

$$\boldsymbol{u}_{(1)} = [\varepsilon_1\ \varepsilon_2\ \varepsilon_3\ \vartheta_{23}\ \vartheta_{12}\ \vartheta_{21}\ \vartheta_{13}\ \vartheta_{22}\ \vartheta_{11}]^T, \tag{5.5}$$

$$\boldsymbol{u}_{(2)} = [e_1^*\ e_2^*\ e_3^*\ \psi_{23}^*\ \psi_{12}^*\ \psi_{21}^*\ \psi_{13}^*\ \psi_{22}^*\ \psi_{11}^*]^T, \tag{5.6}$$

$$\boldsymbol{u}_{(3)} = \boldsymbol{q} = [\boldsymbol{q}_1^T\ \boldsymbol{q}_2^T\ \boldsymbol{q}_3^T]^T, \qquad \boldsymbol{q}_m^T = [x_{1m}^*\ x_{2m}^*\ x_{3m}^*\ \omega_{1m}\ \omega_{2m}] \quad (m = 1, 2, 3), \tag{5.7}$$

where the parenthetic subscripts enumerate the variation levels. Variations in the vector $\boldsymbol{q}$ referred to as the vector of the generalized coordinates represent the degrees of freedom of the element. Using the levels of variable quantities, we obtain the desired coefficients of the variations recursively.

6 Strain energy of the finite element

In the presence of thermal effects, the strain energy of the shell element is expressed in terms of the strain invariants (4.1) as

$$\Pi = \int_F \left[\frac{1}{2}(B_1 I_\varepsilon^2 - 2B_2 I_{\varepsilon\varepsilon}) + \frac{1}{2}\left(D_1 I_\kappa^2 - 2D_2 I_{\kappa\kappa}\right) + G_1 I_\varepsilon I_\kappa - 2G_2 I_{\varepsilon\kappa} + \frac{1}{2}C_\Gamma I_\Gamma - B_T I_\varepsilon - D_T I_\kappa\right] dF, \tag{6.1}$$

where

$$(B_1, G_1, D_1) = \int_{-\frac{h}{2}}^{\frac{h}{2}} (1, z, z^2)\frac{E}{1-\nu^2}\, dz, \qquad (B_2, G_2, D_2) = \int_{-\frac{h}{2}}^{\frac{h}{2}} (1, z, z^2)\frac{E}{1+\nu}\, dz, \tag{6.2}$$

$$C_\Gamma = k\int_{-\frac{h}{2}}^{\frac{h}{2}} G\, dz, \qquad (B_T, D_T) = \int_{-\frac{h}{2}}^{\frac{h}{2}} (1, z)\frac{E}{1-\nu}\alpha\Delta T\, dz. \tag{6.3}$$

Here E is Young's modulus, ν is Poisson's ratio, G is the transverse shear modulus, k is the shear correction factor, α is the coefficient of thermal expansion, and ΔT is the temperature rise. The four first terms in (6.1) represent the membrane and bending strain energies, the fifth and sixth terms takes into account membrane-bending coupling due to nonsymmetrical distribution of mechanical properties about the middle surface of the shell, the seventh term represents the transverse shear strain energy, and the last two terms describe the thermal effects.

According to the first-order shear deformation theory, the shear correction factor appearing in the transverse shear strain energy is introduced to take into account nonuniform distribution of shear stresses through the shell thickness. We calculate this factor by formulas given by Argyris et al. [48] and Vlachoutsis [53]:

$$k = R^2 \left(\int_{-\frac{h}{2}}^{\frac{h}{2}} G\,dz \cdot \int_{-\frac{h}{2}}^{\frac{h}{2}} \frac{t^2(z)}{G}\,dz \right)^{-1}, \qquad R = \int_{-\frac{h}{2}}^{\frac{h}{2}} \frac{E}{1-\nu^2}(z - z_N)^2\,dz, \tag{6.4}$$

$$t(z) = -\int_{-\frac{h}{2}}^{z} \frac{E}{1-\nu^2}(\xi - z_N)\,d\xi, \qquad z_N = \frac{G_1}{B_1}. \tag{6.5}$$

Here z_N is the coordinate of the neutral surface. It is worth noting that the shear correction factor depends on the distribution of the mechanical properties of the material in the normal direction to the shell middle surface. For an isotropic material, formulas (6.4) and (6.5) give $z_N = 0$ and $k = 5/6$.

Substituting strain–displacement relations (5.1) and expressions for the strain invariants (4.1) into (6.1) and using Assumptions 4 and 5 listed in Sect. 2, we write the strain energy of the finite element in matrix notation as

$$\Pi = \frac{1}{2}\boldsymbol{u}_{(1)}^T \boldsymbol{K}\boldsymbol{u}_{(1)} - \boldsymbol{u}_{(1)}^T \boldsymbol{P}, \tag{6.6}$$

where $\boldsymbol{u}_{(1)}$ is the vector given by (5.5), $\boldsymbol{K}$ is the 9×9 symmetric natural stiffness matrix, and $\boldsymbol{P}$ is the nine-component loading vector. The quantities $\boldsymbol{K}$ and $\boldsymbol{P}$ are calculated by the formulas

$$\boldsymbol{K} = \begin{bmatrix} \boldsymbol{K}_\varepsilon & \boldsymbol{K}_{\varepsilon\kappa} \\ \boldsymbol{K}_{\varepsilon\kappa}{}^T & \boldsymbol{K}_\kappa + \boldsymbol{K}_\Gamma \end{bmatrix}, \quad \boldsymbol{P} = \begin{Bmatrix} \boldsymbol{P}_\varepsilon \\ \boldsymbol{P}_\kappa \end{Bmatrix}, \tag{6.7}$$

$$\boldsymbol{K}_\varepsilon = F[B_1 \boldsymbol{\tau}\boldsymbol{\tau}^T - 2B_2(\boldsymbol{\mu}\boldsymbol{\mu}^T - \boldsymbol{\rho})],$$

$$\boldsymbol{K}_{\varepsilon\kappa} = F[G_1 \boldsymbol{\tau}\boldsymbol{\tau}^T - 2G_2(\boldsymbol{\mu}\boldsymbol{\mu}^T - \boldsymbol{\rho})]\boldsymbol{Z},$$

$$\boldsymbol{K}_\kappa = \int_F \boldsymbol{C}^T[D_1 \boldsymbol{\tau}\boldsymbol{\tau}^T - 2D_2(\boldsymbol{\mu}\boldsymbol{\mu}^T - \boldsymbol{\rho})]\boldsymbol{C}\,dF, \tag{6.8}$$

$$\boldsymbol{K}_\Gamma = \boldsymbol{W}^T \boldsymbol{M}\boldsymbol{W}, \ \boldsymbol{P}_\varepsilon = FB_T\boldsymbol{\tau}, \ \boldsymbol{P}_\kappa = D_T\boldsymbol{Z}^T\boldsymbol{\tau}, \tag{6.9}$$

$$\boldsymbol{\tau}^T = 2[aa_1 - 2a_1^2 \quad aa_2 - 2a_2^2 \quad aa_3 - 2a_3^2],$$

$$\boldsymbol{\mu}^T = [a_1 \quad a_2 \quad a_3], \tag{6.10}$$

$$\boldsymbol{\rho} = 2\begin{bmatrix} a_1^2 & 0 & 0 \\ 0 & a_2^2 & 0 \\ 0 & 0 & a_3^2 \end{bmatrix}, \quad \boldsymbol{M} = FC_\Gamma \begin{bmatrix} \tau_1 & 0 & 0 \\ 0 & \tau_2 & 0 \\ 0 & 0 & \tau_3 \end{bmatrix}. \tag{6.11}$$

Here $\boldsymbol{W}$, $\boldsymbol{Z}$, and $\boldsymbol{C}$ are 3×6 matrices whose nonzero entries are given by

$$W_{11} = W_{12} = \eta_{12}, \quad W_{23} = W_{24} = \eta_{22}, \quad W_{35} = W_{36} = \eta_{32}, \tag{6.12}$$

$$Z_{11} = \frac{1}{l_1}, \quad Z_{12} = -\frac{1}{l_1}, \quad Z_{23} = \frac{1}{l_2}, \quad Z_{24} = -\frac{1}{l_2}, \quad Z_{35} = \frac{1}{l_3}, \quad Z_{36} = -\frac{1}{l_3}, \tag{6.13}$$

$$\begin{aligned} C_{11} &= \frac{1}{l_1}[1 + \eta_{11}(L_3 - L_2)], \\ C_{12} &= -\frac{1}{l_1}[1 + \eta_{11}(L_2 - L_3)], \\ C_{23} &= \frac{1}{l_2}[1 + \eta_{21}(L_1 - L_3)], \\ C_{24} &= -\frac{1}{l_2}[1 + \eta_{21}(L_3 - L_1)], \\ C_{35} &= \frac{1}{l_3}[1 + \eta_{31}(L_2 - L_1)], \\ C_{36} &= -\frac{1}{l_3}[1 + \eta_{31}(L_1 - L_2)]. \end{aligned} \tag{6.14}$$

It follows from (6.14) that the components of the 6×6 matrix $\boldsymbol{K}_\kappa$ are quadratic functions of the area coordinates and, hence, the integral over the triangle area in (6.8) can be evaluated exactly by numerical integration using only three Gauss integration points (e.g. [52]).

7 Variations of the strain energy

The total potential energy of the shell element is written as $U = \Pi - A$, where A is the work of the external forces. We write the first and second variations of the strain energy of the shell finite element in terms of variations of the vectors (5.5), (5.6), and (5.7):

$$\delta U = \delta \boldsymbol{u}_{(m)}^T \boldsymbol{g}_{(m)}, \quad \delta^2 U = \delta \boldsymbol{u}_{(m)}^T \boldsymbol{H}_{(m)} \delta \boldsymbol{u}_{(m)}, \tag{7.1}$$

where $\boldsymbol{g}_{(m)}$ and $\boldsymbol{H}_{(m)}$ are the gradient and the Hessian corresponding to the mth variation level, respectively. The values of $\boldsymbol{g} = \boldsymbol{g}_{(3)}$ and $\boldsymbol{H} = \boldsymbol{H}_{(3)}$ required for formulating the equations of equilibrium are computed by the recursive formulas (summation over s):

$$\boldsymbol{g}_{(m+1)} = \boldsymbol{u}'_{(m)} \boldsymbol{g}_{(m)}, \quad \boldsymbol{H}_{(m+1)} = \boldsymbol{u}'_{(m)} \boldsymbol{H}_{(m)} \boldsymbol{u}'^T_{(m)} + g_{(m)s} \boldsymbol{u}''_{(m)s} \quad (m = 1, 2; s = 1, \ldots, 9). \tag{7.2}$$

Here $g_{(m)s}$ is the sth component of the vector $\boldsymbol{g}_{(m)}$ and $\boldsymbol{u}'_{(m)}$ and $\boldsymbol{u}''_{(m)s}$ are the matrices composed of the first and second partial derivatives of the components of the mth level with respect to the components of the $(m+1)$th variation level, respectively. Formulas for calculating the matrices $\boldsymbol{u}'_{(m)}$ and $\boldsymbol{u}''_{(m)s}$ are given in [44]. The computation process (7.2) begins for the initial values

$$\boldsymbol{g}_{(1)} = \boldsymbol{K}\boldsymbol{u}_{(1)} - \boldsymbol{P}, \ \boldsymbol{H}_{(1)} = \boldsymbol{K}. \tag{7.3}$$

The calculation procedure for the element can be summarized as follows:

1. Input the nodal values of the coordinates and normal unit vectors to the shell middle surface.

2. Calculate the initial geometry parameters l_m, F, a, and a_m by formulas (4.2), material properties by formulas (2.1) and matrix $\boldsymbol{K}$ by formulas (6.7)–(6.11).
3. Calculate $\boldsymbol{u}_{(1)}$, $\boldsymbol{g}_{(1)}$, and $\boldsymbol{H}_{(1)}$ by formulas (5.1) and (7.3).
4. Calculate $\boldsymbol{u}_{(2)}$, $\boldsymbol{u}'_{(1)}$, and $\boldsymbol{u}'_{(1)s}(s = 1, \ldots, 9)$ by the formulas given in [44].
5. Calculate $\boldsymbol{u}_{(3)}$, $\boldsymbol{u}'_{(2)}$, and $\boldsymbol{u}''_{(2)s}(s = 1, \ldots, 9)$ by the formulas given in [44].

Once the gradient $\boldsymbol{g} = \boldsymbol{g}_{(3)}$ and the Hessian $\boldsymbol{H} = \boldsymbol{H}_{(3)}$ have been obtained for an individual element, they are assembled into global vectors and matrices of the finite-element assemblage using a standard technique (see, e.g. [52]). In accordance with the Newton–Raphson method, we determine the equilibrium states of the shell by solving iteratively the following system of equations for the variations of the generalized coordinates $\delta\boldsymbol{q}$:

$$\boldsymbol{H}^{p-1}\delta\boldsymbol{q}^{p} + \boldsymbol{g}^{p-1} = 0, \tag{7.4}$$

where $\boldsymbol{H}$ and $\boldsymbol{q}$ are the Hessian and gradient of the total strain energy of the finite-element assemblage, respectively, $\delta\boldsymbol{q}$ is the vector of variations in generalized coordinates, and the superscript denotes the iteration number. The formulas for updating values of the nodal coordinates and direction cosines of the normal vectors can be found in [43,44]. It is worth noting that the first iteration yields the linear solution of the problem.

8 Numerical examples

In this section, the performance of the finite element is numerically verified on some standard test problems. The solutions obtained are compared with those from other finite elements available in literature.

8.1 Brief study of shear locking free behavior

To study locking-free behavior of the proposed element, we consider the linear problem of a functionally graded plate with a span a subjected to uniformly distributed transverse load q. To make transverse shear effects more pronounced, we consider clamped boundary conditions. Young's moduli and Poisson's ratio of the metal and ceramic constituents are as follows: $E_m = 7 \times 10^{10}\,\mathrm{N/m^2}$, $E_c = 38 \times 10^{10}\,\mathrm{N/m^2}$, and $\nu_m = \nu_c = 0.3$. Variation of Young's modulus E across the beam thickness is described by the power law (2.3) in which P is replaced by E. Owing to symmetry of the problem, a quarter of the plate was modeled using mesh types shown in Fig. 2. Dimensionless values of the central deflection of the plate obtained for various span-to-thickness ratios are summarized in Tables 1 and 2 for the power-law exponent $n = 0$ and $n = 5$, respectively. Recall, the case of $n = 0$ corresponds to isotropic ceramic plate. The deflections of isotropic ceramic plates listed in Table 1 agree well with the reference solution of Soh et al. [54]. For $n = 5$, the calculation results are compared to the reference solution obtained by the quadrilateral layered element SHELL181 available in the ANSYS finite element package. For the SHELL181 element, the variation of the elastic properties were approximated by a piecewise constant function using 64 layers and 32×32 mesh for the quarter of the plate. One can see from Tables 1 and 2 that as the span-to-ratio increases to 10^{11}, the effect of the transverse shear strains becomes negligible and the solution approaches a thin-plate limit, which shows that the finite element is shear locking free.

8.2 The effect of elastic property distribution on the shear correction factor

In the analysis of functionally graded plates and shells based on the first order shear deformation theory, it is common approach to take the shear correction factor equal to 5/6, which corresponds to a homogeneous material. We estimate the effect of the shear correction factor dependent on the material properties on the response of FG structures. To this end, we consider a clamped square plate and a spherical panel with square planform subjected to uniformly distributed transverse load q. The plate and panel have the span $a = 0.2\,\mathrm{m}$ and the radius of the spherical shell is taken to be $R = 2a$. We confine our analysis to small deflections. The mechanical characteristics of the plate are $E_m = 7 \times 10^{10}\,\mathrm{N/m^2}$, $E_c = 38 \times 10^{10}\,\mathrm{N/m^2}$, and

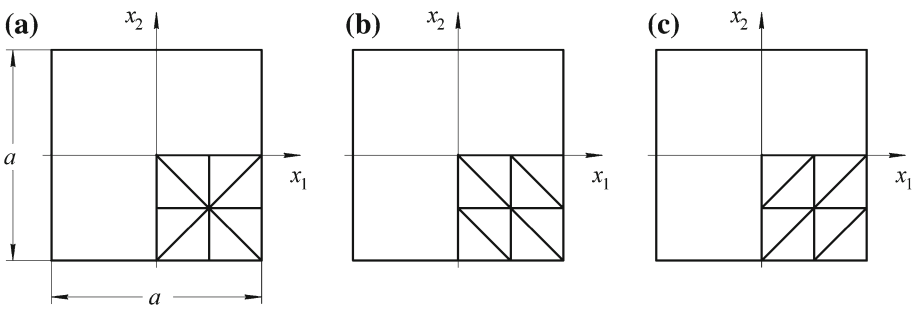

Fig. 2 Square plate and mesh types

Table 1 Mesh convergence for central deflection of a clamped ceramic plate under uniformly distributed load ($n = 0$)

a/h	Mesh type	$100wE_ch^3/[12(1-\nu_c^2)qa^4]$				Soh et al. [54]
		2×2	4×4	8×8	16×16	
5	A	0.2301	0.2200	0.2179	0.2174	0.2167
	B	0.2274	0.2190	0.2175	0.2173	
	C	0.2231	0.2192	0.2177	0.2173	
10	A	0.1675	0.1550	0.1516	0.1507	0.1499
	B	0.1713	0.1551	0.1514	0.1507	
	C	0.1611	0.1541	0.1514	0.1507	
100	A	0.1463	0.1331	0.1284	0.1272	0.1265
	B	0.1566	0.1349	0.1288	0.1270	
	C	0.1406	0.1317	0.1281	0.1271	
10^{11}	A	0.1461	0.1330	0.1282	0.1270	0.1265
	B	0.1565	0.1348	0.1286	0.1270	
	C	0.1404	0.1315	0.1280	0.1269	

Table 2 Mesh convergence for central deflection of a clamped FG plate under uniformly distributed load ($n = 5$)

a/h	Mesh type	$100wE_ch^3/[12(1-\nu_c^2)qa^4]$				Ref. solution
		2×2	4×4	8×8	16×16	
5	A	0.7370	0.7304	0.7298	0.7297	0.7298
	B	0.7229	0.7268	0.7287	0.7294	
	C	0.7166	0.7278	0.7292	0.7296	
10	A	0.4917	0.4811	0.4773	0.4762	0.4759
	B	0.4987	0.4807	0.4765	0.4759	
	C	0.4761	0.4788	0.4768	0.4761	
100	A	0.4015	0.3935	0.3877	0.3862	0.3858
	B	0.4327	0.3981	0.3886	0.3863	
	C	0.3928	0.3894	0.3868	0.3860	
10^{11}	A	0.4006	0.3927	0.3868	0.3852	n/a
	B	0.4322	0.3975	0.3879	0.3855	
	C	0.3920	0.3885	0.3858	0.3850	

$\nu_m = \nu_c = 0.3$. Table 3 lists the coordinate of the neutral surface z_N, shear correction factors k, and central deflections w for various elastic property profiles governed by the volume fraction exponent n which enters Eq. (2.3). For comparison, the deflections are given for two values of k, one of which was set equal to 5/6 and the other was computed by formulas (6.4) taking into account variation of Young's modulus across the thickness according to Eq. (2.3). The results were obtained for a fine 32×32 mesh of type B (see Fig. 2). The percentage errors in determining the central deflection using $k = 5/6$ are given in parentheses. One can see that the error is noticeable for the fraction exponent n ranging from approximately 5 to 10. For thinner plates, the error decreases since the contribution of the transverse shear flexibility to the total flexibility of the plate becomes negligibly small. For the spherical panel, the effect of the shear correction factor on the central deflection is less pronounced. The problem considered shows that, without introducing much error in the deflections of moderately thick FG structures, one can set the shear correction factor equal to 5/6.

8.3 Finite pure bending of a functionally graded beam

We study large displacements of a cantilevered beam of length L, width b, and height h loaded by tip bending moment M. Under these loading conditions, the beam is known to roll up into a perfect circular arc. This problem is commonly used to test nonlinear capabilities of beam, plate, and shells finite elements to simulate arbitrarily large rotations. For a functionally gradient material, the bending moment and the strain energy stored in the beam are written as

Table 3 The effect of the shear correction factor on response of the clamped plate and spherical shell under uniform transverse load

n	z_N/h	k	$100wE_ch^3/[12(1-\nu_c^2)qa^4]$			
			Plate		Spherical panel ($R/a=2$)	
			$a/h=5$	$a/h=10$	$a/h=5$	$a/h=10$
0.1	0.019	5/6	0.2385 (0.3%)	0.1664 (0.1%)	0.2066 (0.2%)	0.1115 (0%)
		0.839	0.2378	0.1662	0.2061	0.1115
0.5	0.075	5/6	0.3203 (0.5%)	0.2282 (0.2%)	0.2788 (0.4%)	0.1500 (0.1%)
		0.846	0.3186	0.2278	0.2776	0.1498
1	0.115	5/6	0.4081 (−0.1%)	0.2945 (−0.1%)	0.3565(−0.1%)	0.1909 (−0.1%)
		0.830	0.4086	0.2947	0.3568	0.1910
2	0.149	5/6	0.5254 (−3.0%)	0.3781 (−1.1%)	0.4633 (−2.1%)	0.2481 (−0.4%)
		0.769	0.5410	0.3823	0.4734	0.2490
5	0.152	5/6	0.6676 (−8.5%)	0.4594 (−3.6%)	0.5988 (−6.3%)	0.3189 (−1.8%)
		0.678	0.7296	0.4759	0.6393	0.3246
10	0.120	5/6	0.7712 (−8.3%)	0.5146 (−3.5%)	0.6931 (−6.8%)	0.3678 (−1.9%)
		0.690	0.8407	0.5329	0.7399	0.3748
20	0.079	5/6	0.8819 (−5.2%)	0.5849 (−2.1%)	0.7870 (−4.0%)	0.4182 (−1.1%)
		0.741	0.9299	0.5976	0.8201	0.4231
40	0.046	5/6	0.9845 (−2.3%)	0.6594 (−0.9%)	0.8700 (%)	0.4647 (−0.5%)
		0.790	1.0080	0.6657	0.8860	0.4670

$$M=\frac{bD_1}{R}\left(1-\frac{G_1^2}{B_1D_1}\right),\quad \Pi=\frac{M^2L}{bD_1}\left(1-\frac{G_1^2}{B_1D_1}\right)^{-1}, \tag{8.1}$$

where R^{-1} is the curvature of the center line of the beam and the quantities B_1, G_1, and D_1 are given by (6.2). The parenthetic terms in (8.1) account for the fact that the neutral line does not pass through the cross-sectional centroid because of variation of the mechanical properties across the beam thickness. Bearing in mind that the length of the neutral line remains unchanged in pure bending, we obtain the following expressions for the axial and transverse tip displacements:

$$u=L\left(1-\frac{R}{L}\sin\frac{L}{R-z_N}\right),\quad w=R\left(1-\cos\frac{L}{R-z_N}\right), \tag{8.2}$$

where z_N is given by (6.5).

To demonstrate nonlinear capabilities of the finite element, we consider the functionally graded beam represented by only two elements and set $L=1\,\text{m}, b=1\,\text{m}, h=0.001\,\text{m}$, $E_m=0.7\times10^{11}\,\text{N/m}^2$, $E_c=1.51\times10^{11}\,\text{N/m}^2$, and $\nu_m=\nu_c=0$. Figure 3 shows the strain energy and tip displacements versus the bending moment for the volume fraction exponent $n=5$ which enters (2.3). The two-element model with ten degrees of freedom describes very well the finite bending of the beam and fails to converge only when the bending moment attains approximately 12.9 Nm, which corresponds to the rotation of the beam tip through an angle of approximately 100°.

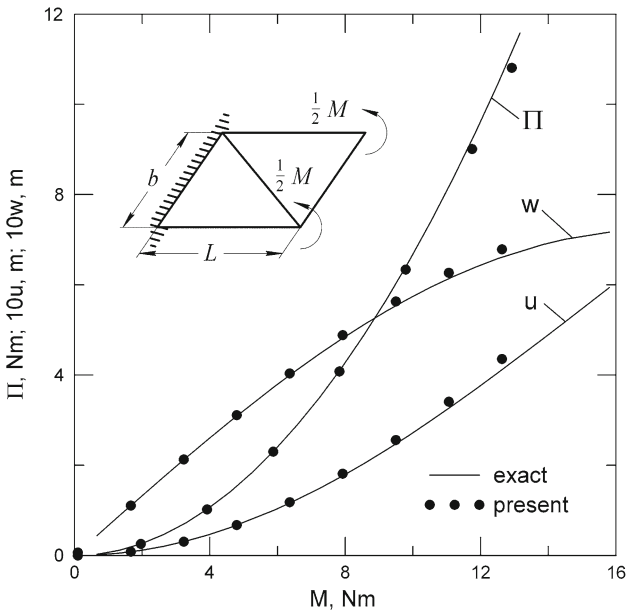

Fig. 3 Strain energy and tip displacements versus bending moment for the functionally graded plate ($n=5$)

Now we study the effect of material property distribution on finite bending using an example of a cantilevered functionally graded beam with $L=12\,\text{m}, b=1\,\text{m}$, and $h=0.1\,\text{m}$, $E_m=0.7\times10^{11}\,\text{N/m}^2$, $E_c=1.51\times10^{11}\,\text{N/m}^2$, and

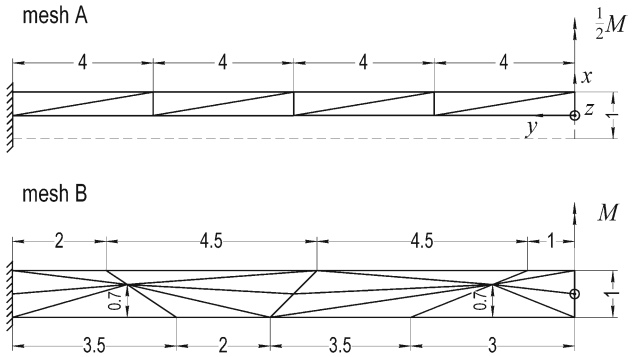

Fig. 4 Beam in pure bending: regular mesh and distorted mesh

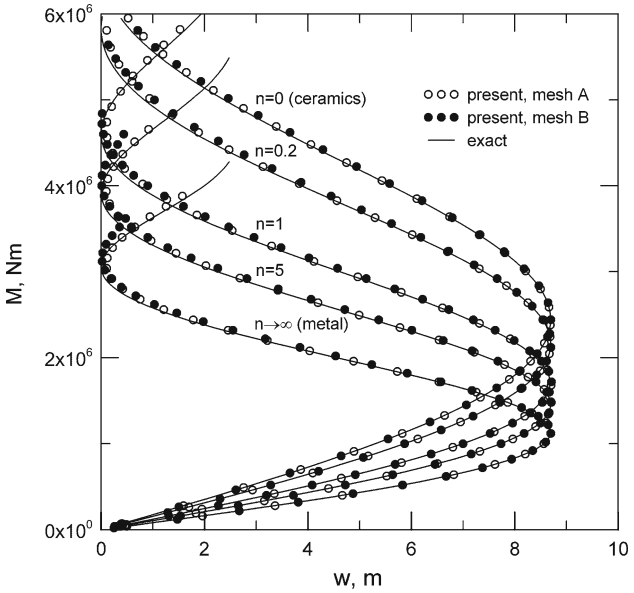

Fig. 5 Moment versus transverse tip displacement of the FG beam in pure bending

$\nu_m = \nu_c = 0$. To obtain the moment–displacement curves, we use mesh patterns shown in Fig. 4. The bending moment versus the tip transverse deflection is shown in Fig. 5 for various values of the fraction exponents n. One can see that the numerical results are in excellent agreement with the theoretical solution given by formulas (8.1) and (8.2). The curves obtained for the distorted mesh shown in Fig. 4 deviate only slightly from the theoretical solution in the region of very large curvature changes where the beam is rolled up into a full circle.

8.4 Square plate under transverse load

A simply supported square plate is subjected to transverse uniformly distributed load q. The lower surface of the plate is purely metal (aluminum) and the upper surface is purely ceramic (alumina). Boundary conditions are such that deflection and rotation along the boundary vanish (hard support, see e.g. [52]) and in-plane displacements are allowed (movable

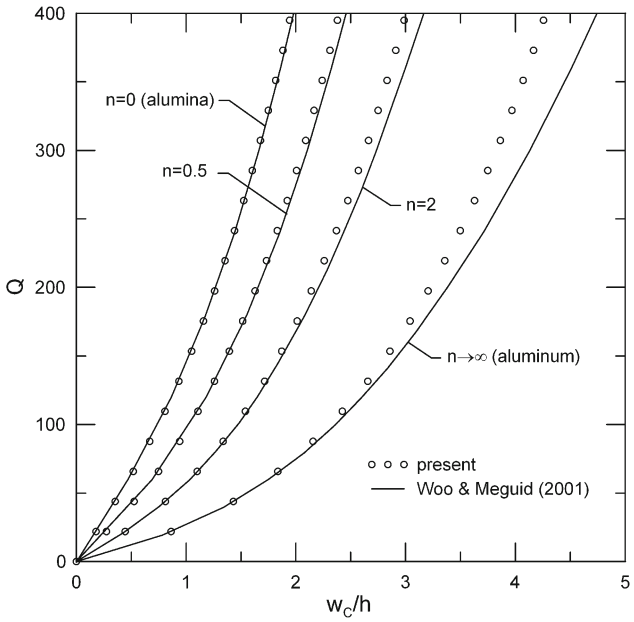

Fig. 6 Load versus central deflection of simply supported square FG plates under uniform load

support). Geometrical and mechanical characteristics of the plate are as follows: span $a = 0.2$ m, thickness $h = 0.01$ m, Poisson's ratios $\nu_m = \nu_c = 0.3$, and Young's moduli $E_m = 7 \times 10^{10}$ N/m^2 and $E_c = 38 \times 10^{10}$ N/m^2.

To study nonlinear behavior of the functionally graded plate, we use an 8×8 Union-Jack mesh (see Fig. 2a). Figure 6 shows the dimensionless load $Q = qa^4/(E_m h^4)$ versus the dimensionless central deflection w_C/h for various values of the volume fraction exponent n. The calculation results are compared with the solution of [13] based on the von Karman strain–displacement relations. One can see that the results agree well for moderately large deflections. The difference between the solutions becomes pronounced when the central deflection exceeds the plate thickness by approximately a factor of 3. This can be attributed to the fact that large transverse deflections accompanied by considerable in-plane displacements are beyond the range of applicability of the von Karman relations.

8.5 Axisymmetric buckling of circular plates

A circular ceramic–metal plate of radius R is compressed by uniform radial load q. We determine the buckling load under the clamped boundary conditions. The buckling problem is solved in fully geometrically nonlinear formulation with allowance for the prebuckling deformation of the plate. The critical loads are determined using the condition that the determinant of the Hessian in Eq. (7.4) vanishes. The constituents of the materials are aluminum and alumina with Young's moduli $E_m = 0.7 \times 10^{11}$N/m^2, and $E_c = 3.8 \times 10^{11}$N/m^2, respectively. For both constituents,

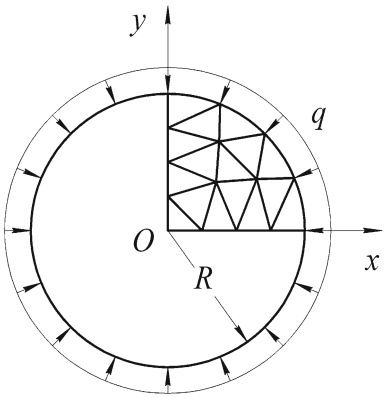

Fig. 7 Circular plate under uniform compression and mesh pattern

Poisson's ratio is assumed to be constant and equal to 0.3. The thickness-to-radius ratio h/R is equal to 0.1, where $h = 0.1$ m. The finite-element results were obtained for a quarter of the plate using the mesh pattern where each side of the quarter is divided into m segments (see Fig. 7). For the clamped plate, the bifurcation-type buckling behavior is observed. The reason is that the bending moments generated by the in-plane compressive load are neutralized by the support reacting moments such that the plate remains flat in the prebuckling state. Table 4 lists the critical load q_{cr} for various values of the volume fraction index n. The present solution exhibits monotonic mesh convergence and agrees well with the data of [38,55].

8.6 Buckling of cylindrical shells under compressive load

We consider the buckling problem of a simply supported functionally graded cylindrical shell subjected to axial compressive load q (Fig. 8). The parameters of the shell are as follows: $R = 0.1$ m, $L = 0.1$ m, $h = 0.001$ m, $E_m = 2.0104 \times 10^{11}$ N/m^2, $\nu_m = 0.3262$, $E_c = 3.4843 \times 10^{11}$ N/m^2, and $\nu_c = 0.24$. We evaluate the critical load q_{cr} assuming that buckling modes are symmetrical about the xz plane. It should be noted that prebuckling deformation is taken into account. The half of the shell is modeled by a uniform Union-Jack mesh with 20 elements in the axial direction and 64 elements in the circumferential direction. Two cases are studied: (1) case C where the outer surface of the shell is ceramic rich and the inner surface is metal rich and (2) case M where the outer surface of the shell is metal rich and the inner surface is ceramic rich. Table 5 lists the dimensionless coordinate z_N/h of the neutral surface, critical load q_{cr}, and critical end shortening u_z for various values of the exponent n in the power law (2.3). Setting $n = 0$, we obtain two limiting cases of purely ceramic shell for case C and purely metal shell for case M. For linear variation of the material properties across the shell thickness ($n = 1$), Figs. 9 and 10 show the buckling modes for cases C and M, respectively. The modes are characterized by nine waves in the circumferential direction and three halfwaves in the axial direction. One can see that the wave amplitudes decay from the loaded end in axial direction. The reason is that the loaded section $z = 0$ is allowed to warp and distort, whereas the section $z = L$ is assumed to remain planar, circular, and inextensible. For case M, the decay is very much pronounced and the critical load is slightly higher compared to case C. An increase in the critical load for case M can be attributed to the fact that the neutral surface is shifted toward the inner ceramic rich surface. Hence, the end load applied with eccentricity to the neutral surface tends to diminish the prebuckling axisymmetric expansion which occurs under axial compression of the shell due to Poisson's effect.

8.7 Thermal buckling and postbuckling of functionally graded plates

In this section, thermal buckling and postbuckling behavior of fully clamped square Al_2O_3–Ni plates subjected to uniform temperature rise is analyzed. For simplicity, we assume that the thermal load is uniform through the plate thickness and the properties of the FG plates do not depend on temperature. The span-to-thickness ratio and wall thickness are taken to be $a/h = 50$ and $h = 0.02$ m, respectively. The material properties of the constituents are as follows [56]: $E_c = 3.93 \times 10^{11}$ N/m^2, $\nu_c = 0.25$, and $\alpha_c = 0.88 \times 10^{-5}\,^{\circ}$C^{-1} for Al_2O_3 and $E_m = 1.995 \times 10^{11}$ N/m^2, $\nu_m = 0.3$, and $\alpha_m = 1.33 \times 10^{-5}\,^{\circ}$C^{-1} for Ni. For this problem, a quarter

Table 4 Buckling compressive loads q_{cr} for clamped FG circular plates for $R/h = 10$

Mesh parameter, m	Number of elements	$q_{cr} \times 10^{-8}$(N/m)		
		$n = 0$	$n = 0.5$	$n = 2$
4	16	4.4987	2.9542	1.8124
8	64	4.8332	3.1531	1.8998
16	256	4.9199	3.2043	1.9219
32	1,024	4.9414	3.2170	1.9275
Najafizadeh and Heydari [38]		4.97467361	3.23407504	1.94235302
Hong et al. [55]		4.93352	–	–

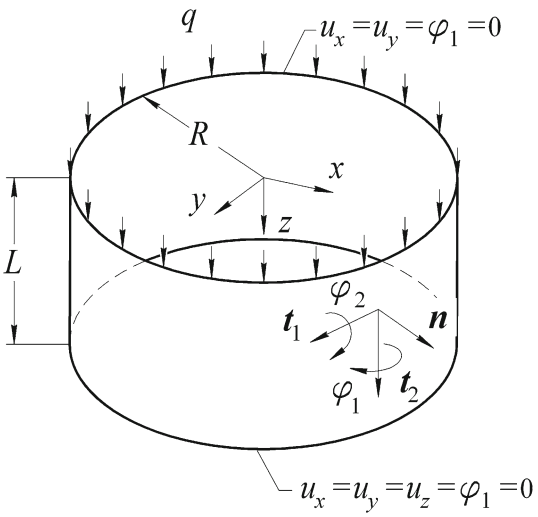

Fig. 8 Simply supported cylindrical shell under compressive load

Fig. 9 First buckling mode of the compressed simply supported cylindrical shell with ceramic outer surface and metal inner surface ($n = 1$)

Fig. 10 First buckling mode of the compressed simply supported cylindrical shell with metal outer surface and ceramic inner surface ($n = 1$)

of the plate was modeled using the mesh type shown in Fig. 2a. Table 6 lists the data on mesh convergence of the critical temperature rise as a function of the volume fraction exponent n. In this case, the bifurcation-type buckling behavior is observed, which supports the findings of [21]. The results on the critical temperature rise are compared with the data obtained using a quadrilateral layered finite element SHELL181 available in the package ANSYS. In this case, a 40×40 mesh for a quarter of the plate was used and continuous variation of the thermomechanical properties of the functionally graded material was approximated by piecewise constant variation using 32 layers.

Figure 11 shows the postbuckling behavior of the Al_2O_3–Ni square plate under uniform temperature rise for $a/h = 100$. The present finite-element solution found by using the 8×8 Union-Jack mesh for a quarter of the plate (see Fig. 2a) is compared with the curves of [56] obtained by a solid finite element with 18 degrees of freedom. According to the present solution, the plates exhibit softer response. For the isotropic plates, the results compared differ by approximately 10%. For verification, additional calculations were performed by the finite element SHELL43 of ANSYS using 20×20 mesh. The resulting load–deflection curve in Fig. 11 is in excellent agreement with the present solution.

9 Conclusions

A nonconventional approach based on the natural-strain invariants and the concept of kinematic group has been applied to develop a curved triangular finite element for geometrically nonlinear analysis of shear deformable functionally graded shells. A computational benefit offered by the invariant-based approach is that no operations on coordinate transformation are required since no local coordinates are introduced for the elements. The main results presented in the paper can be summarized as follows.

Table 5 Critical loads and end shortenings for the simply supported cylindrical shell under compression

n	z_N/h		$q_{cr} \times 10^{-6}$, (N/m)		$u_{z,cr} \times 10^3$ (m)	
	Case *C*	Case *M*	Case *C*	Case *M*	Case *C*	Case *M*
0	0	0	1.979	1.142	0.568	0.568
0.5	0.0328	−0.0393	1.535	1.299	0.517	0.524
1	0.0447	−0.0447	1.386	1.393	0.511	0.513
2	0.0491	−0.0410	1.276	1.504	0.518	0.508
5	0.0389	−0.0271	1.199	1.663	0.537	0.516

Table 6 Critical temperature rise for the clamped FG square plate for $a/h = 50$

Mesh	ΔT (°C)				
	$n = 0$	$n = 0.5$	$n = 1$	$n = 2$	$n \to \infty$
2×2	142.00	116.85	110.16	106.94	88.72
4×4	151.85	124.92	117.48	114.10	96.17
8×8	156.10	128.43	120.87	117.43	99.12
16×16	157.19	129.84	122.89	119.84	99.93
32×32	157.20	129.85	122.90	119.85	99.93
ANSYS	157.73	129.74	121.70	117.94	100.30

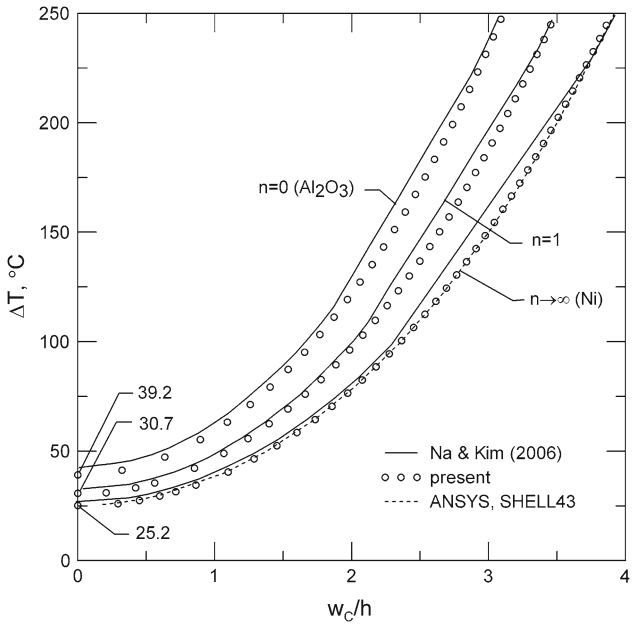

Fig. 11 Temperature rise versus postbuckling deflection of the clamped square plate

1. Simple expressions for the natural-strain invariants have been obtained to determine the strain energy of a triangular finite element of a functionally graded shell.
2. Compact and easily programmable formulas have been given to compute the gradient and Hessian of the finite element of a shear deformable functionally graded shell.
3. The effect of the material properties on the shear correction factor and response of the functionally graded plates has been studied; the effect was found to show up for moderately thick plates when the exponent n in the power law distribution ranges from approximately 5 to 10.

The finite element proposed has excellent nonlinear bending characteristics, but its shortcoming is that membrane and transverse shear strains are constant. The finite element is shear locking free and can be used in the analysis of thin and moderately thick functionally graded shells undergoing large elastic displacements and rotations.

Acknowledgments The authors acknowledge the use of ANSYS v.11 through an educational software license No. 00435880.

References

1. Koizumi M (1993) The concept of FGM. Ceramic Transactions Functionally Gradient Materials 34:3–10
2. Chi S, Chung Y (2006) Mechanical behavior of functionally graded material plates under transverse load—part I: analysis. Int J Solids Struct 43:3657–3674
3. Chi S, Chung Y (2006) Mechanical behavior of functionally graded material plates under transverse load—part II: numerical results. Int J Solids Struct 43:3675–3691
4. Navazi HM, Haddadpour H, Rasekh M (2006) An analytical solution for nonlinear cylindrical bending of functionally graded plates. Thin Walled Struct 44:1129–1137
5. Ghannadpour SAM, Alinia MM (2006) Large deflection behavior of functionally graded plates under pressure loads. Compos Struct 75:67–71
6. Samsam Shariat BA, Javaheri R, Eslami MR (2005) Buckling of imperfect functionally graded plates under in-plane compressive loading. Thin Walled Struct 43:1020–1036
7. Samsam Shariat BA, Eslami MR (2006) Thermal buckling of imperfect functionally graded plates. Int J Solids Struct 43:4082–4096
8. Javaheri R, Eslami MR (2002) Buckling of functionally graded plates under in-plane compressive loading. Z Angew Math Mech 82:277–283
9. Javaheri R, Eslami MR (2002) Thermal buckling of functionally graded plates. AIAA J 40:162–169
10. Yang J, Shen HS (2003) Non-linear analysis of functionally graded plates under transverse and in-plane loads. Int J Non Linear Mech 38:467–482
11. Ma LS, Wang TJ (2003) Nonlinear bending and post-buckling of a functionally graded circular plate under mechanical and thermal loadings. Int J Solids Struct 40:3311–3330
12. Najafizadeh MM, Eslami MR (2002) Buckling analysis of circular plates of functionally graded materials under uniform radial compression. Int J Mech Sci 44:2479–2493
13. Woo J, Meguid SA (2001) Nonlinear analysis of functionally graded plates and shallow shells. Int J Solids Struct 38:7409–7421
14. Huang HW, Han Q (2009) Nonlinear elastic buckling and postbuckling of axially compressed functionally graded cylindrical shells. Int J Mech Sci 51:500–507

15. Huang HW, Han Q (2010) Research on nonlinear postbuckling of functionally graded cylindrical shells under radial loads. Compos Struct 92:1352–1357
16. Wu L, Jiang ZQ, Liu J (2005) Thermoelastic stability of functionally graded cylindrical shells. Compos Struct 70:60–68
17. Yang J, Liew KM, Wu YF, Kitipornchai S (2006) Thermo-mechanical post-buckling of FGM cylindrical panels with temperature-dependent properties. Int J Solids Struct 43:307–324
18. Li SR, Batra RC (2006) Buckling of axially compressed thin cylindrical shells with functionally graded middle layer. Thin Walled Struct 44:1039–1047
19. Praveen GN, Reddy JN (1998) Nonlinear transient thermoelastic analysis of functionally graded ceramic-metal plates. Int J Solids Struct 35((33):4457–4476
20. Croce LD, Venini P (2004) Finite elements for functionally graded Reissner–Mindlin plates. Comput Methods Appl Mech Eng 193:705–725
21. Navazi HM, Haddadpour H (2008) Nonlinear cylindrical bending analysis of shear deformable functionally graded plates under different loadings using analytical methods. Int J Mech Sci 50: 1650–1657
22. Wu L (2004) Thermal buckling of a simply supported moderately thick rectangular FGM plate. Compos Struct 64:211–218
23. Prakash T, Singha MK, Ganapathi M (2008) Thermal postbuckling analysis of FGM skew plates. Eng Struct 30:22–32
24. Prakash T, Singha MK, Ganapathi M (2009) Influence of neutral surface position on the nonlinear stability behavior of functionally graded plates. Comput Mech 43:341–350
25. Wu TL, Shukla KK, Huang JH (2007) Post-buckling analysis of functionally graded rectangular plates. Compos Struct 81:1–10
26. Shen HS (2009) Functionally graded materials: nonlinear analysis of plates and shells. CRC Press, Boca Raton
27. Shen HS (2007) Thermal postbuckling behavior of shear deformable FGM plates with temperature-dependent properties. Int J Mech Sci 49:466–478
28. Park JS, Kim JH (2006) Thermal postbuckling and vibration analyses of functionally graded plates. J Sound Vib 289:77–93
29. Aydogdu M (2008) Conditions for functionally graded plates to remain flat under in-plane loads by classical plate theory. Compos Struct 82:155–157
30. Nosier A, Fallah F (2009) Nonlinear analysis of functionally graded circular plates under asymmetric transverse loading. Int J Non Linear Mech 44: 928–942. doi:10.1016/j.ijnonlinmec.2009.07.001
31. Santos H, Mota Soares CM, Mota Soares CA, Reddy JN (2009) A semi-analytical finite element model for the analysis of cylindrical shells made of functionally graded materials. Compos Struct 91:427–432
32. Ganesan N, Kadoli R (2004) Studies on linear thermoelastic buckling and free vibration analysis of geometrically perfect hemispherical shells with cut-out. J Sound Vib 277:855–879
33. Bhangale RK, Ganesan N, Padmanabhan C (2006) Linear thermoelastic buckling and free vibration behavior of functionally graded truncated conical shells. J Sound Vib 292:341–371
34. Zhao X, Liew KM (2009) Geometrically nonlinear analysis of functionally graded shells. Int J Mech Sci 51:131–144
35. Arciniega RA, Reddy JN (2007) Large deformation analysis of functionally graded shells. Int J Solids Struct 44:2036–2052
36. Nguyen TK, Sab K, Bonnet G (2008) First-order shear deformation plate models for functionally graded materials. Compos Struct 83:25–36
37. Reddy JN (2000) Analysis of functionally graded plates. Int J Numer Methods Eng 47:663–684
38. Najafizadeh MM, Heydari HR (2008) An exact solution for buckling of functionally graded circular plates based on higher order shear deformation plate theory under uniform radial compression. Int J Mech Sci 50:603–612
39. Li XY, Ding HJ, Chen WQ (2006) Pure bending of simply supported circular plate of transversely isotropic functionally graded material. J Zhejiang Univ Sci A 7(8):1324–1328
40. Li XY, Ding HJ, Chen WQ (2008) Elasticity solutions for a transversely isotropic functionally graded circular plate subject to an axisymmetric transverse load qr^k. Int J Solids Struct 45:191–210
41. Cheng ZQ, Batra RC (2000) Deflection relationships between the homogeneous Kirchhoff plate theory and different functionally graded plate theories. Arch Mech 52:143–158
42. Vel SS, Batra RC (2002) Exact solution for thermoelastic deformations of functionally graded thick rectangular plates. AIAA J 40:1421–1433
43. Kuznetsov VV, Levyakov SV (2007) Phenomenological invariant-based finite-element model for geometrically nonlinear analysis of thin shells. Comput Methods Appl Mech Eng 196:4952–4964
44. Kuznetsov VV, Levyakov SV (2008) Geometrically nonlinear shell finite element based on the geometry of a planar curve. Finite Elem Anal Des 44:450–461
45. Kuznetsov VV, Levyakov SV (2009) Phenomenological invariants and their application to geometrically nonlinear formulation of triangular finite elements of shear deformable shells. Int J Solids Struct 46:1019–1032
46. Argyris JH, Tenek L (1994) A practicable and locking-free laminated shallow shell triangular element of varying and adaptable curvature. Comput Methods Appl Mech Eng 119:215–282
47. Argyris JH, Tenek L (1996) Natural mode method: a practicable and novel approach to the global analysis of laminated composite plates and shells. Appl Mech Rev 49:381–399
48. Argyris J, Tenek L, Olofsson L (1997) TRIC: a simple but sophisticated 3-node triangular element based on 6 rigid-body and 12 straining modes for fast computational simulations of arbitrary isotropic and laminated composite shells. Comput Methods Appl Mech Eng 145:11–85
49. Bian ZG, Chen WQ, Lim CW, Zhang N (2005) Analytical solutions for single- and multi-span functionally graded plates in cylindrical bending. Int J Solids Struct 42:6433–6456
50. Kuznetsov VV, Levyakov SV (1994) Kinematic groups and finite elements in deformable body mechanics. Izv Ross Akad Nauk Mekh Tverd Tela 3:67–82 (in Russian)
51. Zhao ZF, Chen WJ (1995) New finite element model for analysis of Kirchhoff plate. Int J Num Methods Eng 38:1201–1214
52. Zienkiewicz OC (1977) The finite element method in engineering science. McGraw-Hill, London
53. Vlachoutsis S (1992) Shear correction factors for plates and shells. Int J Num Methods Eng 33:1537–1552
54. Soh AK, Long ZF, Cen S (1999) A new nine DOF triangular element for analysis of thick and thin plates. Comput Mech 24: 408–417
55. Hong GM, Wang CM, Tan TJ (1993) Analytical buckling solutions for circular Mindlin plates: inclusion of inplane prebuckling deformation. Arch Appl Mech 63:534–542
56. Na KS, Kim JH (2006) Thermal postbuckling investigations of functionally graded plates using 3-D finite element method. Finite Elements Anal Des 42:749–756